TÜBİTAK

Turkish Journal of Chemistry

http://journals.tubitak.gov.tr/chem/

Research Article

Turk J Chem
(2014) 38

doi:10.3906/kim-1207-37

Simulation of impedance spectra of oxalic acid electroreduction to glyoxylic acid: effect of chemical activator, pH, activation energy, and reduction potential

Niyazi Alper TAPAN*
Department of Chemical Engineering, Faculty of Engineering, Gazi University, Ankara, Turkey

Received: 17.07.2012 • **Accepted:** 14.07.2013 • **Published Online:** 16.12.2013 • **Printed:** 20.01.2014

Abstract: The aim of this study was to examine qualitatively the effect of important electrochemical parameters on the faradaic impedance spectra of oxalic acid electroreduction. The impedance spectrum of a 3-step oxalic acid electroreduction mechanism was simulated by the solution of a faradaic impedance equation based on 3 state variables. Before the solution of the faradaic impedance equation, the electroreduction mechanism was analyzed and it was seen that this mechanism can be represented by an electrical circuit composed of 2 resistors and a capacitance or inductance. The effect of chemical activator on the impedance spectrum was determined by using the relation between topological indices and electrode potential given in the literature. Simulation results indicated that the increase in the alkyl chain length in the chemical activator has a minor effect on the charge transfer resistance. On the other hand, pH drop could have a significant effect on the reduction in charge transfer resistance. In addition, inductive behavior can be seen if the electroreduction of adsorbed oxalic acid becomes the rate limiting step.

Key words: Oxalic acid, glyoxylic acid, electroreduction, impedance

1. Introduction

Glyoxylic acid is known to be an important intermediate in many sectors of the chemical industry like perfumery, pharmaceuticals, and fine chemicals. Although the best-known route for the production of glyoxylic acid is by electroreduction of oxalic acid, there are still limitations regarding the commercialization of the process because of the fast deactivation of the cathode by early hydrogen evolution, the use of low hydrogen overvoltage metals, and metal ion deposition.[1] Therefore, in order to prevent deactivation of the cathode by side reactions, some alternatives have been proposed, such as addition of quaternary ammonium salts and tertiary amines to the catholyte or use of high hydrogen overvoltage cathodes like lead.[2] The cations (quaternary ammonium salts and tertiary amines) that are used for reactivation of the cathode electrode were seen to change the mechanism of reduction by protecting the cathode electrode after adsorption to the surface. The adsorption and coverage of activator molecule is greatly affected by the molecular structure, which changes the double layer structure and the potential of reduction.

2. Relation of topological indices of activators and electroreduction potential

The activation ability of activator molecular structures can be predicted quantitatively by using topological indices. Electrode potential can be determined by Eq. (1) below, which includes topological indices (A_{m1}, A_{m2}, A_{m3}):

*Correspondence: atapan@gazi.edu.tr

$$E = X_o + X_1.A_{m1} + X_2.A_{m2} + X_3.A_{m3} \quad (1)$$

The constants X_o, X_1, X_2, and X_3 in Eq. (1) were determined from the relation between current efficiency Y and topological indices by using the Butler–Volmer relation given in Eq. (2):[3]

$$Y = z.F.k^{\theta}.C'_{Ox}.C'^{2}_{H+}.I_0^{-1}.Exp(-\alpha zFE/RT) \quad (2)$$

In Eq. (2), C'_{OX} and C'_{H+} represent oxalic acid and proton concentration and I_o and k^{θ} represent the overall current density (including desired and side reactions) and pre-exponential factor. If the current efficiency in Eq. (2) is recorded for different activators, the constants in Eq. (2) can be determined by nonlinear regression of Eq. (3), which represents the relation of current efficiency and topological indices.

$$\ln Y = A + B.(X_o + X_1.A_{m1} + X_2.A_{m2} + X_3.A_{m3}) \quad (3)$$

After determination of the constants in Eq. (3) the potential dependence on the topological indices of activators can be determined:

$$E = -0.2536 + 0.000286.A_{m1} - 0.000181.A_{m2} - 0.000028.A_{m3} \quad (4)$$

The electroreduction potentials that were calculated using Eq. (4) for different activators can be seen in Table 1.

Table 1. Topological indices of activators and their electrode potentials.

Activator	A_{m1}	A_{m2}	A_{m3}	E(V)
$C_4H_{12}NCl$	10.08695	24.21825	0	–0.2551
$C_8H_{20}NBr$	17.9155	30.0055	54.2513	–0.25543
$C_{16}H_{36}NBr$	33.0042	45.6026	65.3323	–0.25424
$C_{16}H_{36}NCl$	33.0042	45.6026	65.3323	–0.25424
$C_{32}H_{68}NBr$	63.2222	70.9455	86.686	–0.25079
$C_{19}H_{42}NBr$	38.59605	46.636	51.88	–0.25246
$C_{16}H_{36}NI$	33.0042	45.6026	65.3323	–0.25424
$C_{16}H_{36}NOH$	33.0042	45.6026	65.3323	–0.25424
$C_4H_{12}NOH$	10.08695	24.21825	0	–0.2551
$C_8H_{20}NOH$	17.9155	30.0055	54.2413	–0.25543
$C_{19}H_{42}NCl$	42.0925	59.3784	74.4705	–0.25439
$C_{16}H_{36}N_2O_3$	33.0042	45.6026	65.3323	–0.25424

3. Three-step electroreduction mechanism

The electroreduction mechanism of oxalic acid was presented by a 3-step mechanism (Eqs. (5)–(7)).[4] The mechanism consists of 2 electron transfer steps and 1 chemical step. These are the electrosorption of bulk oxalic acid, electroreduction of methyldioxy, carboxy intermediate, and formation of glyoxylic acid. In Eqs. (5) and (6), M represents the metal cathode.

$$HOOCCOOH + H^+ + e^- + M \rightarrow HOOCC(OH)_2M \quad (5)$$

$$HOOCC(OH)_2M + e^- \rightarrow HOOCC(OH)_2^- + M \quad (6)$$

$$HOOCC(OH)_2^- + H^+ \rightarrow HOOCCHO + H_2O \quad (7)$$

4. Method of approach

4.1. Derivation of faradaic current based on the 3-step mechanism

Based on the 3-step mechanism given above in Eqs. (5)–(7), initially the rates of change of surface and bulk species were derived using Butler–Volmer relations:

$$\frac{d\theta_1}{dt} = -k_1.\theta_1.C_{H+}.(1-\theta_2).(a.n.F/q).\exp(\beta_1.n_1.F.E/(RT)) \tag{8}$$

$$\frac{d\theta_2}{dt} = k_1.\theta_1.C_{H+}.(1-\theta_2).(a.n.F/q).\exp(\beta_1.n_1.F.E/(RT)) - k_2.\theta_2.\exp(\beta_2.n_2.F.E/(RT)) \tag{9}$$

$$\frac{d\theta_3}{dt} = k_2.\theta_2.\exp(\beta_2.n_2.F.E/(RT)) - k_3.\theta_3.C_{H+}.(a.n.F/q).\exp(-E_a/(RT)) \tag{10}$$

$$\frac{dC_{H+}}{dt} = -k_1.\theta_1.C_{H+}.(1-\theta_2).\exp(\beta_1.n_1.F.E/(RT)) - k_3.\theta_3.C_{H+}.(a.n.F/q).\exp(-E_a/(RT)) \tag{11}$$

$$\frac{dC_{GLY}}{dt} = k_3.\theta_3.C_{H+}.\exp(-E_a/(RT)) \tag{12}$$

In Eqs. (8)-(12), θ_1 denotes the concentration of oxalic acid converted into surface coverage per area of electrode, θ_2 denotes the surface coverage of adsorbed species $HOOCC(OH)_2M$, θ_3 denotes the concentration of ionic species $HOOCC(OH)_2^-$ in terms of surface coverage per area of electrode, C_{H^+} denotes the concentration of protons, and C_{GLY} denotes the concentration of glyoxylic acid.

The conversion of bulk concentration of oxalic acid into surface concentration per area of electrode (surface concentration) was done by using the relation given below:

$$\theta_1 = C_{OX} \times a \times n \times F/q \tag{13}$$

In Eq. (13) above, q is the charge for a monolayer coverage, 210 $\mu C/cm^2$, and a is the ratio of volume of the cell to electrode area (cm^3/cm^2).

By the use of the rate of change of species θ_1 and θ_2 given in Eqs. (8)–(12), the faradaic current density of oxalic acid reduction can be derived as seen in Eq. (14):

$$I_F = q.(k_1\theta_1 C_{H+}(1-\theta_2)\left(a.n.\frac{F}{q}\right)\exp\left(\beta_1.n_1.F.\frac{E}{R.T}\right) + k_2\theta_2\exp\left(\beta_2.n_2.F.\frac{E}{R.T}\right)) \tag{14}$$

4.2. Steady state parameters

For the mathematical modeling of faradaic impedance of irreversible electrode reactions given in the proposed mechanism, initially the faradaic current is expressed as a function of potential and state variables. According to Eq. (14), the state variables are θ_1, C_{H+}, and θ_2, and so the faradaic current can be expressed as a function of 3 state variables and potential (Eq. (15)):

$$I_F = f(E, \theta_1, C_{H+}, \theta_2) \tag{15}$$

If faradaic current is expressed as a deviation variable from steady state,

$$\Delta I_F = \left(\frac{\partial I_F}{\partial E}\right)_{ss}.\Delta E + \left(\frac{\partial I_F}{\partial \theta_1}\right)_{ss}.\Delta\theta_1 + \left(\frac{\partial I_F}{\partial C_{H+}}\right)_{ss}\Delta C_{H+} + \left(\frac{\partial I_F}{\partial \theta_2}\right)_{ss}.\Delta\theta_2 \tag{16}$$

Therefore, the faradaic admittance is

$$\frac{\Delta I_F}{\Delta E} = \left(\frac{\partial I_F}{\partial E}\right)_{ss} + m_1\left(\frac{\Delta\theta_1}{\Delta E}\right) + m_2\left(\frac{\Delta C_{H+}}{\Delta E}\right) + m_3\left(\frac{\Delta\theta_2}{\Delta E}\right) \tag{17}$$

$$\frac{\Delta I_F}{\Delta E} = \frac{1}{Z_F} = Y_F = \frac{1}{R_t} + \sum m_i \frac{\Delta\theta_i}{\Delta E} \tag{18}$$

In Eq. (18), R_t and m_i denote the charge transfer resistance and derivative of faradaic current with respect to state variables at steady state,

$$m_1 = \left(\frac{\partial I_F}{\partial\theta_1}\right)_{ss} m_2 = \left(\frac{\partial I_F}{\partial C_{H+}}\right)_{ss} m_3 = \left(\frac{\partial I_F}{\partial\theta_2}\right)_{ss} \tag{19}$$

If a sinusoidal input in terms of complex function is applied to the reduction potential, then the output functions, which are concentrations and coverages, can also be expressed as complex functions as follows:

$$\Delta E = |\Delta E|\, exp\,(jwt) \tag{20}$$

$$\Delta\theta = |\Delta\theta|\, exp\,(jwt) \tag{21}$$

Then the rate of change of coverage species can also be expressed as complex functions,

$$\frac{d\Delta\theta}{dt} = |\Delta\theta|\, exp\,(jwt)\, jw \tag{22}$$

$$\frac{d\Delta\theta}{dt} = \Delta\theta jw \tag{23}$$

All $\Delta\theta_i/\Delta E$ terms in the faradaic admittance term can be expressed in terms of other deviation variables at steady state as follows:

$$jw\frac{\Delta\theta_i}{\Delta E} = b_i + \sum_{k=1}^{3} J_{ik}\frac{\Delta\theta_k}{\Delta E} \tag{24}$$

$$J_{ik} = \left(\frac{\partial\theta_i}{\partial\theta_k}\right)_{SS} \qquad i,k = 1,2,3 \tag{25}$$

$$\partial b_i = \left(\frac{\partial\dot{\theta}_i}{E}\right)_{SS} \qquad i,k = 1,2,3 \tag{26}$$

$$jw\frac{\Delta\theta_1}{\Delta E} = \left(\frac{\partial\dot{\theta}_i}{\partial E}\right)_{SS} + \frac{\partial\dot{\theta_1}}{\partial\theta_1}\frac{\Delta\theta_1}{\Delta E} + \frac{\partial\dot{\theta_1}}{\partial C_{H+}}\frac{\Delta C_{H+}}{\Delta E} + \frac{\partial\dot{\theta_1}}{\partial\theta_2}\frac{\Delta\theta_2}{\Delta E} \tag{27}$$

$$jw\frac{\Delta C_{H+}}{\Delta E} = \left(\frac{\partial\dot{C_{H+}}}{\partial E}\right)_{SS} + \frac{\partial\dot{C_{H+}}}{\partial\theta_1}\frac{\Delta\theta_1}{\Delta E} + \frac{\partial\dot{C_{H+}}}{\partial C_{H+}}\frac{\Delta C_{H+}}{\Delta E} + \frac{\partial\dot{C_{H+}}}{\partial\theta_2}\frac{\Delta\theta_2}{\Delta E} \tag{28}$$

$$jw\frac{\Delta\theta_2}{\Delta E} = \left(\frac{\partial\dot{\theta}_2}{\partial E}\right)_{SS} + \frac{\partial\dot{\theta_2}}{\partial\theta_1}\frac{\Delta\theta_1}{\Delta E} + \frac{\partial\dot{\theta_2}}{\partial C_{H+}}\frac{\Delta C_{H+}}{\Delta E} + \frac{\partial\dot{\theta_2}}{\partial\theta_2}\frac{\Delta\theta_2}{\Delta E} \tag{29}$$

Finally, the faradic admittance term can be completely expressed as a function of deviation variables at steady state:

$$\frac{\Delta I_F}{\Delta E} = \frac{1}{Z_F} = Y_F = \frac{1}{R_t} + \left(\frac{\partial I_F}{\partial \theta_1}\right)_{SS}\left(\frac{1}{jw}.\left[\left(\frac{\partial \dot{\theta}_i}{\partial E}\right)_{SS} + \frac{\partial \dot{\theta_1}}{\partial \theta_1}\frac{\Delta\theta_1}{\Delta E} + \frac{\partial \dot{\theta_1}}{\partial C_{H+}}\frac{\Delta C_{H+}}{\Delta E} + \frac{\partial \dot{\theta_1}}{\partial \theta_2}\frac{\Delta\theta_2}{\Delta E} + \left(\frac{\partial \dot{C_{H+}}}{\partial E}\right)_{SS}\right.\right.$$

$$\left.\left. + \frac{\partial \dot{C_{H+}}}{\partial \theta_1}\frac{\Delta\theta_1}{\Delta E} + \frac{\partial \dot{C_{H+}}}{\partial C_{H+}}\frac{\Delta C_{H+}}{\Delta E} + \frac{\partial \dot{C_{H+}}}{\partial \theta_2}\frac{\Delta\theta_2}{\Delta E} + \left(\frac{\partial \dot{\theta_2}}{\partial E}\right)_{SS} + \frac{\partial \dot{\theta_2}}{\partial \theta_1}\frac{\Delta\theta_1}{\Delta E} + \frac{\partial \dot{\theta_2}}{\partial C_{H+}}\frac{\Delta C_{H+}}{\Delta E} + \frac{\partial \dot{\theta_2}}{\partial \theta_2}\frac{\Delta\theta_2}{\Delta E}\right]\right) \tag{30}$$

If Eq. (30) above is arranged to separate real and imaginary parts, Eq. (31) can be obtained as shown below:

$$\frac{1}{Z_f} = \frac{1}{Rt} + \frac{A' + j\omega\beta C + \omega^2\beta^2 B}{D - j\omega\beta S - \omega^2\beta^2 T + j\omega^3\beta^3} \tag{31}$$

In Eq. (31) the parameters A', C, B, D, S, T include steady state parameters, which were defined by Ahlberg et al.[5] When Eq. (31) is separated into real and imaginary parts in order to obtain Nyquist diagrams and Bode plots, the final form of the faradaic impedance equation can be obtained.

4.3. Determination of steady state parameters

In order to determine the steady state parameters in the faradaic impedance equation (Eq. (31)), time dependent coverage and concentration equations (Eqs. (8)–(12)) were solved simultaneously by using the stiff numerical algorithm in the Polymath ordinary differential equation solver. For the simulation of change in surface coverages, θ_1,θ_2,θ_3 and bulk concentration of protons and glyoxylic acid, model parameters given in Table 2, were used.

Table 2. Model parameters.

Model parameter	Value
Electrode radius (r)	0.5 cm
Cell volume (V)	40 cm^3
Monolayer charge (q)	210 $\mu C/cm^2$
Volume/Area ratio (a)	203 cm^3/cm^2
Initial oxalic acid concentration (C_{OX})	1 M
Cell temperature (T)	298 K
Initial proton concentration (C_{H+})	0.5 M
Pre-exponential factor (k_1, k_2, k_3)	[a] 9 × 10^{-22} cov^{-2} s^{-1}
Transfer coefficient (β)	0.5
Activation energy (E_a)	10,000 J/mol [a]

[a] The magnitudes were approximated from Scott et al.[6,7]

In Table 2, the approximate magnitude of the pre-exponential factor used in the model was obtained by conversion of 15.85 × 10^{-12} mol^{-2} s^{-1} $(m^3)^3/(m^2)$ (taken from Scott et al.) to 9 × 10^{-22} cov^{-2} s^{-1} after multiplying it by $(100^7)/F^2 \times q^2 \times (1/a)^3$.[6,7]

4.4. Determination of possible equivalent electrical circuit for the electroreduction mechanism

Initially, in order to determine the possible equivalent electrical circuit that can represent the 3-step electroreduction mechanism, all the static species (which are known to be at high concentrations in electrolyte solution,

and so their mass transfer limitations are negligible and their surface concentrations are assumed to be constant) are eliminated from the mechanism. As seen from the mechanism below, the third step is completely eliminated because it involves static species.

$$e^- + M \rightarrow HOOCC(OH)_2M \tag{32}$$

$$HOOCC(OH)_2M + e^- \rightarrow M \tag{33}$$

After the elimination of static species from the mechanism, the stoichiometric matrix (Eq. (32)) was determined. The stoichiometric matrix is known to be composed of rows that are labeled by the species (e, M, BM (HOOCC(OH)$_2$M)), columns that are labeled by the reactions (rxn1, rxn2, rxn3), and entries that are stoichiometric coefficients of the species.[8]

$$\begin{matrix} rxn1 & rxn2 & rxn3 \end{matrix}$$

$$\left[\begin{array}{ccc|c} -1 & -1 & 0 & e \\ -1 & 1 & 0 & M \\ 1 & -1 & 0 & BM \end{array}\right] \tag{34}$$

The rank or complexity of the stoichiometric matrix indicates the number of independent reactions. This value also shows the number of resistors in the electrical circuit. In Eq. (34), the rank of the matrix (I) is 2 and so there are 2 resistors in the circuit.

In order to understand if inductive behavior exists for this mechanism, the sign of the overall matrix was analyzed. The overall matrix Q is composed of elementary matrices of reaction 1 and 2 as given in Eq. (35).[8–10]

$$\begin{matrix} & Rxn1 & & & Rxn2 \\ e^- + M \rightarrow HOOCC(OH)_2M & & & HOOCC(OH)_2M + e^- \rightarrow M & & \end{matrix}$$

$$Q = \left[\begin{array}{ccc} + & + & - \\ + & + & - \\ - & - & + \end{array}\right] \quad + \quad \left[\begin{array}{ccc} + & - & + \\ - & + & - \\ + & - & + \end{array}\right] \tag{35}$$

Since there are conflicting signs of the 2 elementary matrices (2 independent reactions), there is a possibility of inductive behavior in the mechanism.

In addition to the inductive behavior, in order to see if there is a DC path in the circuit (if the low frequency limit is resistive, the intercept is on the real axis), the possibility of an electron transfer step from static species was analyzed:

$$HOOCCOOH + 2H^+ + 2e^- \rightarrow HOOCCHO + H_2O \tag{36}$$

The above electrochemical step proves that there is a DC path in the circuit, and so X = 2, which means that an additional reaction can be formed that includes both static species and electrons. Therefore, there are 2 resistors in the circuit and there are I + 1 – X/2 capacitors or inductors. Since one of the capacitors is double layer capacitance there is only one capacitor or inductor possible in the faradaic impedance.[10]

Therefore, after determination of the number of resistors and capacitors or inductors, the possible representative electrical circuit diagrams that have DC paths can be shown in Figure 1a and 1b. The equivalent circuits shown in Figure 1 were also presented before for the representation of faradaic impedance for the case of electrochemical reactions involving one adsorbed species.[11]

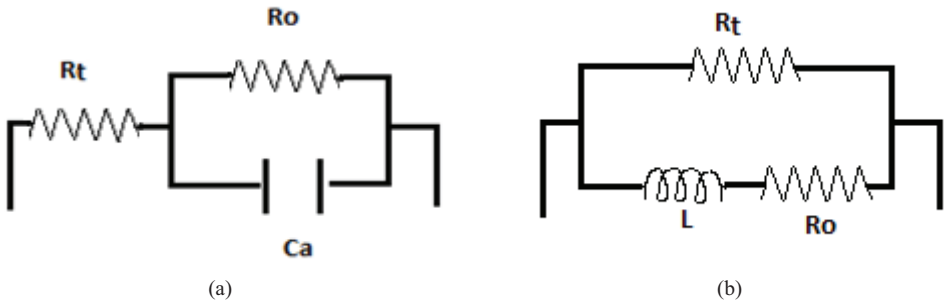

Figure 1. Representative electrical circuits for the 3-step electroreduction mechanism, a) electrical circuit that involves capacitance (Randles circuit) b) electrical circuit that involves inductive behavior.

5. Results and discussion

By the use of the parameters given in Table 2 in order to determine steady state parameters in the faradaic impedance equation (Eq. (31)), electrochemical impedance spectroscopy simulations were performed to investigate the effect of chemical activators, pH, and activation energy of the chemical step (step 3) in the electroreduction mechanism (Eq. (7)), and reduction potential on the behavior of the electroreduction process.

5.1. Effect of chemical activator

In order to determine the effect of chemical activator, topological indices of activators and electrode potentials given in Table 1 were used. Figures 2–4 show Nyquist, Bode, and modulus plots between 0.1 Hz and 1 MHz frequency.

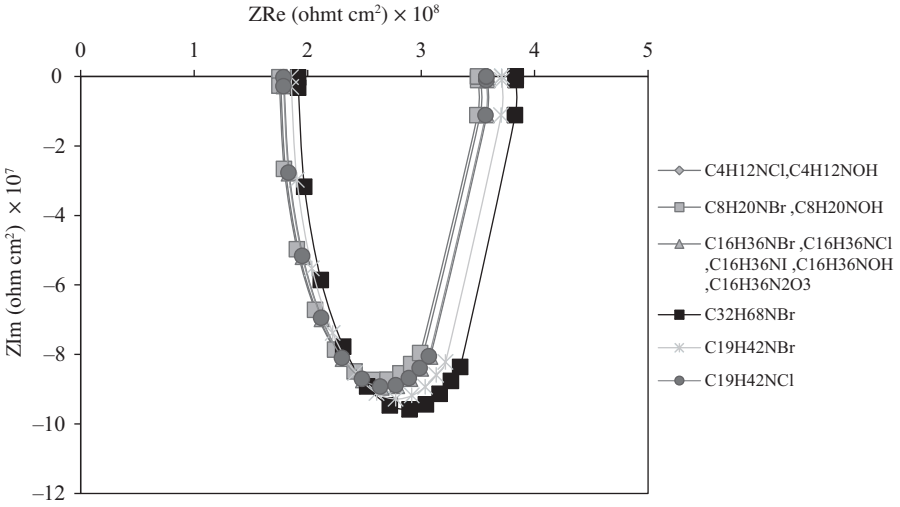

Figure 2. Nyquist plots which show chemical activator effect. Selected parameters for the simulation of impedance spectra: Ea = 10,000 J/mol, C_{H+} = 0.5 M, k = 9 × 10^{-22} cov^{-2} s^{-1}, C_{OX} = 0.5 M.

One important point to note in the Nyquist plots is that as the frequency approaches 1 MHz the real part or the resistance value increases; in fact, in this study, the real axis shows the absolute values for the real part of the impedance (although it is computed as negative). During the simulation of faradaic impedance, the charge transfer resistance for the reduction reaction was actually computed as a negative value since $(\partial E/\partial I)_{SS}$

is negative in magnitude if cathodic current is taken as a positive quantity (increase in the negative potential increases the value of cathodic current). Therefore, for the electrical circuits proposed, if charge transfer resistance is negative due to the reason explained above and if R_o is a positive value, then as frequency approaches higher frequencies like 1 MHz, impedance approaches the value of charge transfer resistance (which is negative) and so the absolute value of the real axis will be more positive compared to the value when frequency approaches zero. Of course, for this condition, in the electrical circuit the absolute value of the charge transfer resistance R_{ct} should be greater than R_o (like in our case).

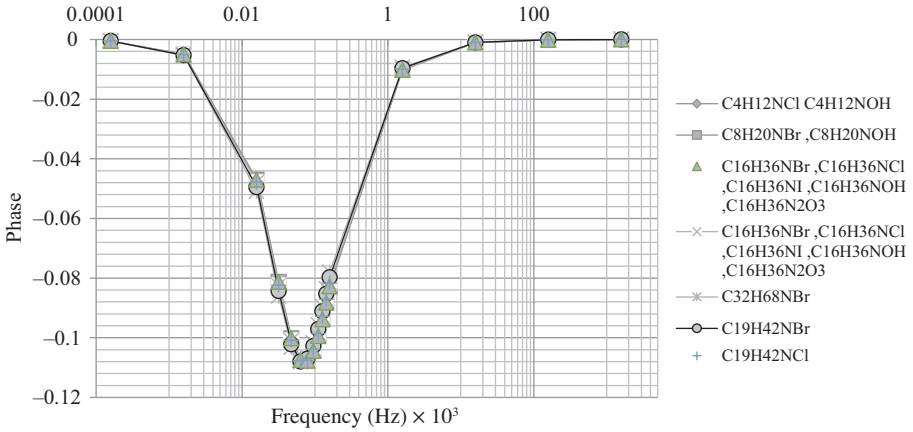

Figure 3. Bode plots showing chemical activator effect. Selected parameters for the simulation of impedance spectra: Ea = 10,000 J/mol, C_{H+} = 0.5 M, k = 9 × 10^{-22} cov^{-2} s^{-1}, C_{OX} = 0.5 M.

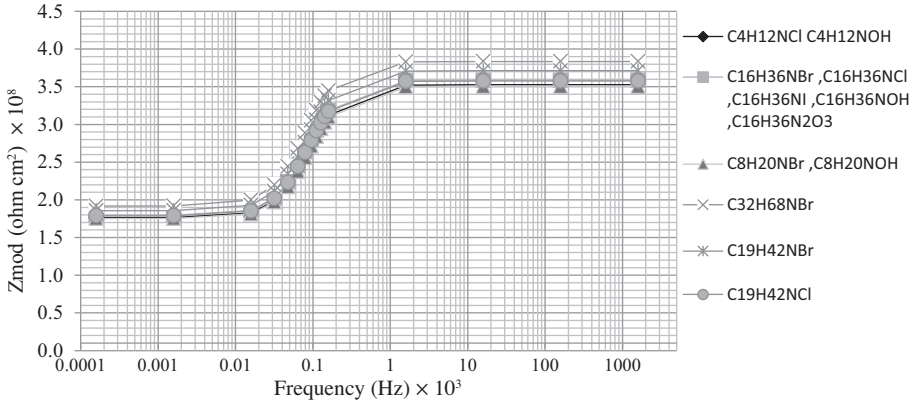

Figure 4. Modulus plots showing chemical activator effect. Selected parameters for the simulation of impedance spectra: Ea = 10,000 J/mol, C_{H+} = 0.5 M, k = 9 × 10^{-22} cov^{-2} s^{-1}, C_{OX} = 0.5 M.

As seen in Figure 2, the diameter of the arc increases with the increase in alkyl chain length in the chemical activator. The increase in the diameter of the arc is associated with the increase in the charge transfer resistance lowering the electrocatalytic activity for electroreduction. The same behavior in the Nyquist plot can also be observed in the modulus plot, which shows an increase in the resistance at higher frequencies. No significant change in the phase angle (which is given as $n\pi$) is seen in Figure 3, which indicates that capacitance effect is negligible.

5.2. Effect of pH

When the proton concentration was changed, a drastic effect on the impedance spectra was observed. The Nyquist plot in Figure 5 shows that the capacitive loop was reduced significantly by increasing proton concentration. At much higher proton concentrations the impedance loop becomes insignificant when compared with the loops at lower proton concentrations. The reduction in the impedance loop with increasing proton concentration indicates that the magnitudes of both charge transfer resistance and capacitance in the electrical circuit drop. The drop in the magnitudes of capacitance can be observed in the Bode plots by the shift in maximum phase angle to higher frequencies (Figure 6). The modulus plots in Figure 7 also show the change in the representative electrical circuit with increasing proton concentration from parallel-series type (Randles circuit) (which is given in Figure 1a) to a single resistance type. If we take a closer look at the Nyquist plot in Figure 5, it is seen that as the proton concentration increases the high and low frequency limits of the loop decrease together with the size of the capacitive loop. Therefore, it can be said that the proton concentration increases the rate of electroreduction as well as decreasing the magnitude of the interfacial capacitance. If the relation of faradaic impedance with the frequency in Eq. (31) is analyzed, it is seen that there would be a complex relationship between interfacial capacitance, the parallel resistance, and the proton concentration. This can be explained by the formulation of faradaic impedance based on the electrical circuit proposed in Figure 1a as shown in Eqs. (38) and (38):[11]

$$Zf = Rt + \frac{1}{\frac{1}{Ra} + jw.Ca} \tag{37}$$

$$Ra = \frac{Rt^2\,|A1|}{A2 - Rt\,|A1|}, \quad Ca = \frac{1}{Rt^2.\,|A1|} \tag{38}$$

Here in Eq. (38) both Ra and Ca depend on charge transfer resistance (which is a function of proton concentration) and state variables like proton concentration (Eq. (15)). A1 and A2 in Eq. (38) denote some kinetic parameters that also depend on state variables.[11] Thus it can be concluded that both the capacitive terms and resistive terms are affected by proton concentration. The increase in proton concentration not only will decrease charge transfer resistance but also will decrease Ca and Ra terms; this is the reason why purely resistive behavior was seen at high proton concentration.

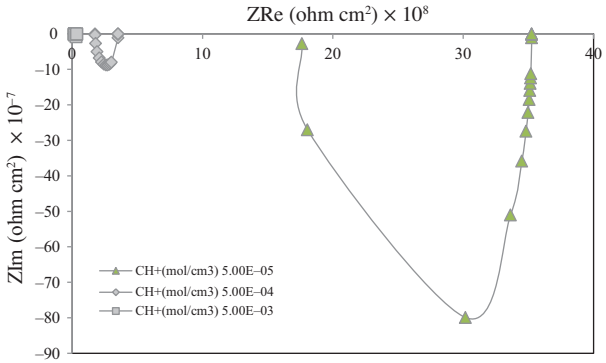

Figure 5. Nyquist plots showing pH effect. Selected parameters for the simulation of impedance spectra: Ea = 10,000 J/mol, k = 9 × 10^{-22} cov^{-2} s^{-1}, C_{OX} = 0.5 M, E = –0.2551 V.

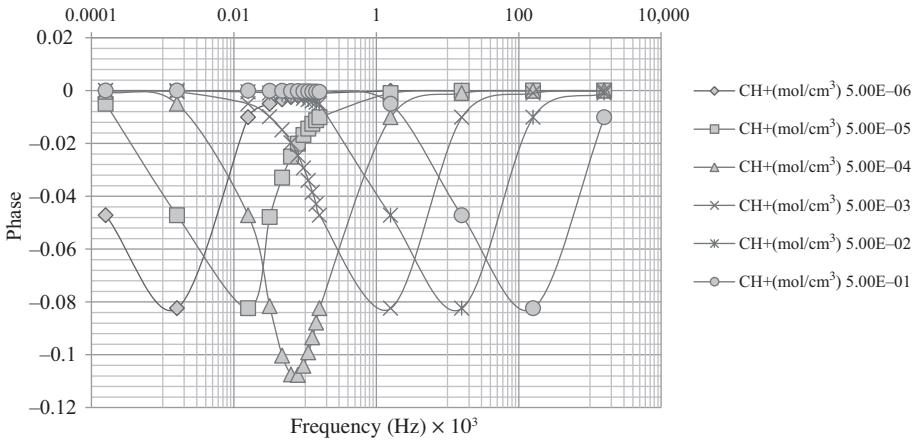

Figure 6. Bode plots showing pH effect. Selected parameters for the simulation of impedance spectra: Ea = 10,000 J/mol, k = 9 × 10^{-22} cov^{-2} s^{-1}, C_{OX} = 0.5 M, E = –0.2551 V.

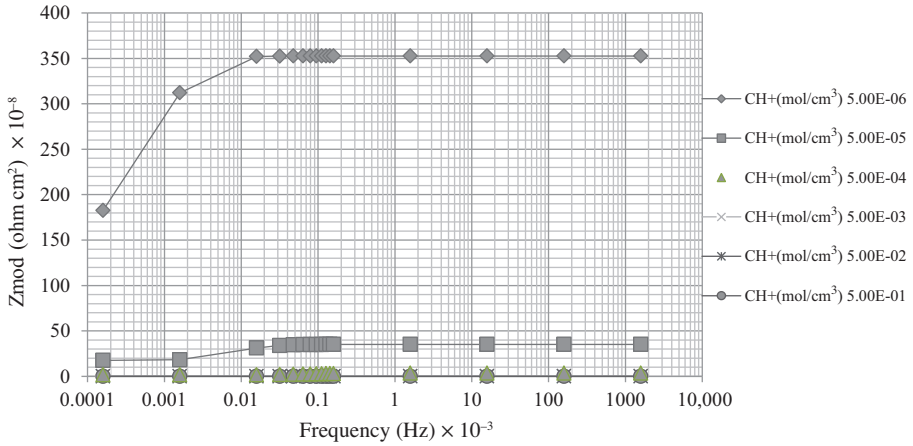

Figure 7. Modulus plots showing pH effect. Selected parameters for the simulation of impedance spectra: Ea = 10,000 J/mol, k = 9 × 10^{-22} cov^{-2} s^{-1}, C_{OX} = 0.5 M, E = –0.2551 V.

5.3. Effect of activation energy

In order to understand the effect of the chemical step (Eq. (7)) in the electroreduction mechanism, activation energy of the ionic reaction was changed to observe its effect on the impedance spectra. As can be seen in the Nyquist plots, there is a possibility of inductive behavior when the activation energy of ionic reaction is lowered. It is also seen that the representative electrical circuit changes from parallel-series type to R–C series or R–L series type. The occurrence of inductive behavior may be related to the limiting behavior of electroreduction of adsorbed oxalic acid.

In order to see the degree of inductive behavior at lower frequencies, Bode and modulus plots were also analyzed. As can be seen in Figures 8 and 9, small inductive behavior starts when the activation energy is lowered by 50% from 100,000 J/mol to 50,000 J/mol (from 5 to 4 orders of magnitude). Above 50,000 J/mol, capacitive behavior takes over induction. Although the capacitive behavior is not seen in the modulus and Bode plots shown in Figures 10–12, the Nyquist plots indicate capacitive behavior (series R–C circuit) at higher activation energy.

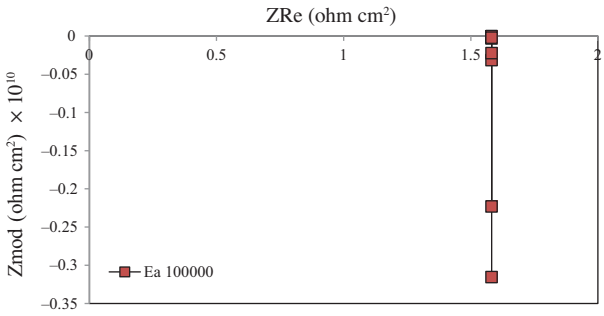

Figure 8. Nyquist plots showing the effect of activation energy. Capacitive behavior is seen. Selected parameters for the simulation of impedance spectra: k = 1 × 10^{-6} cov^{-2} s^{-1}, C_{H+} = 0.5 M, E = –0.2551 V, C_{OX} = 0.5 M.

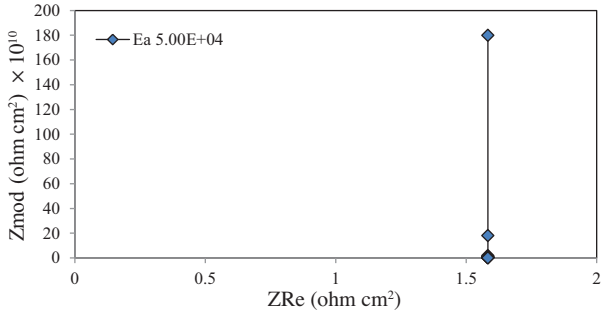

Figure 9. Nyquist plots showing the effect of activation energy. Inductive behavior is seen. Selected parameters for the simulation of impedance spectra: k = 1 × 10^{-6} cov^{-2} s^{-1}, C_{H+} = 0.5 M, E = –0.2551 V, C_{OX} = 0.5 M.

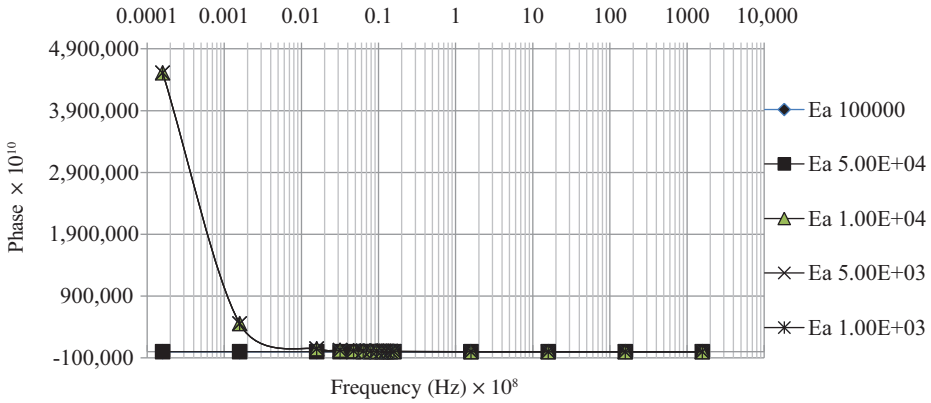

Figure 10. Bode plots showing the effect of activation energy. Selected parameters for the simulation of impedance spectra: k = 1 × 10^{-6} cov^{-2} s^{-1}, C_{H+} = 0.5 M, E = –0.2551 V, C_{OX} = 0.5 M.

Figure 9 demonstrates that the electroreduction mechanism can also be represented by impedance (positive) above the real axis. In fact, this inductive behavior does not mean that magnetic fields occur when the kinetics exhibit inductive behavior. Like in the case of a hydrogen oxidation mechanism involving electrochemical adsorption/desorption, a kinetic mechanism that is independent of the magnetic field can be characterized by inductors.[12,13] In general, induction may occur in langmuirian adsorption mechanisms at some specific condition, for example at a specific set of rate constants that are dependent on potential or activation energy like in our proposed 3-step mechanism. Under the other conditions affecting these rate constants, the

circuit may not involve an inductor. It was previously shown that mechanisms with single adsorbed species can exhibit inductive behavior if the mechanism involves adsorbed species both on the same side of the reaction with the electrons and on the opposite side of electrons in the reaction.[8,14] The condition for inductive behavior in such a kind of mechanism is that the charge transfer resistance is higher than polarization resistance, Rt > Rp. It is known that polarization resistance is the overall resistance at zero frequency (when there are no capacitive or inductive effects) or in other words the overall rate is faster than the rate of electron transfer steps. In this study, it was observed that at lower activation energy when the rate of chemical step is increased, the charge transfer resistance starts to dominate the mechanism and this condition may explain the presence of inductive behavior.

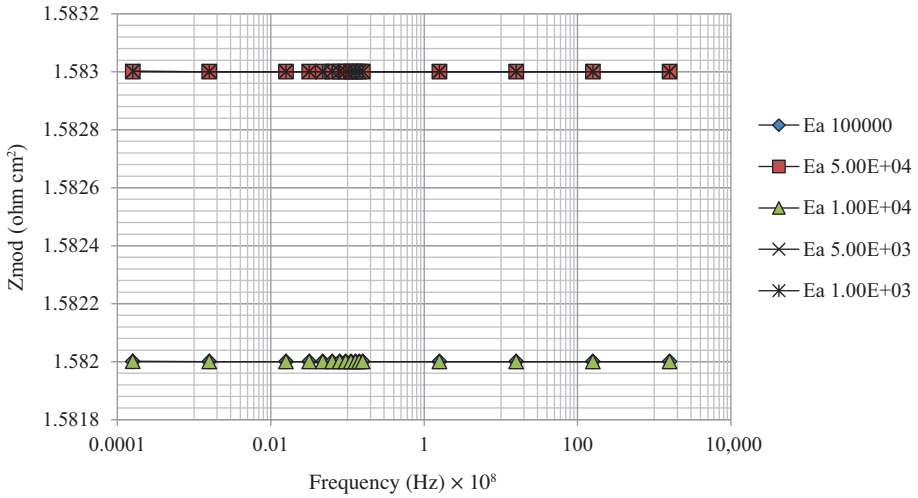

Figure 11. Modulus plots showing the effect of activation energy. Selected parameters for the simulation of impedance spectra: k = 1 × 10^{-6} cov^{-2} s^{-1}, C_{H+} = 0.5 M, E = –0.2551 V, C_{OX} = 0.5 M.

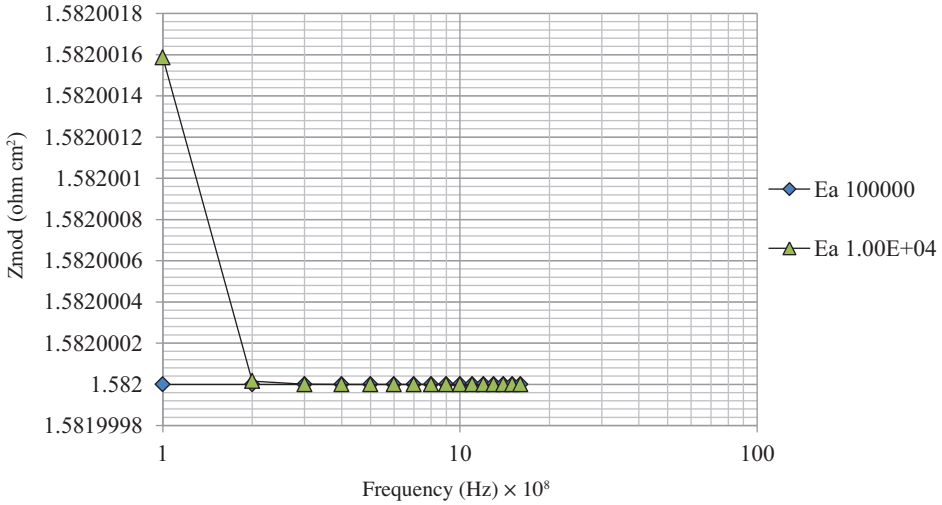

Figure 12. Modulus plots showing the effect of activation energy. Selected parameters for the simulation of impedance spectra: k = 1 × 10^{-6} cov^{-2} s^{-1}, C_{H+} = 0.5 M, E = –0.2551 V, C_{OX} = 0.5 M.

5.4. Effect of reduction potential

The effect of electroreduction potential can be seen in Figures 13–15. As the reduction potential is increased, the capacitive loop almost diminishes in the Nyquist plot (Figure 13). The capacitive loop in Figure 13 is a depressed semicircle rather than a perfect one. In a Randles cell in which there is a perfect capacitor, the Nyquist plot gives a perfect semicircle with low and high frequency limits indicating the resistance elements in the cell. On the other hand, imperfections in the capacitor change the shape of the semicircle. These imperfections can be caused by distribution of time constants for different charge transfer reactions in the electrochemical mechanism.[15,16] Therefore, the capacitive element in the electrical circuit can be a constant phase element (CPE). By the use of CPE parameters shown in Eq. (39),[11] a depressed semicircle can be represented easily.

$$Z_{CPE} = \frac{1}{T(jw)^{\emptyset}} \tag{39}$$

In Eq. (39), T and φ represent constants related to the type of capacitive behavior.

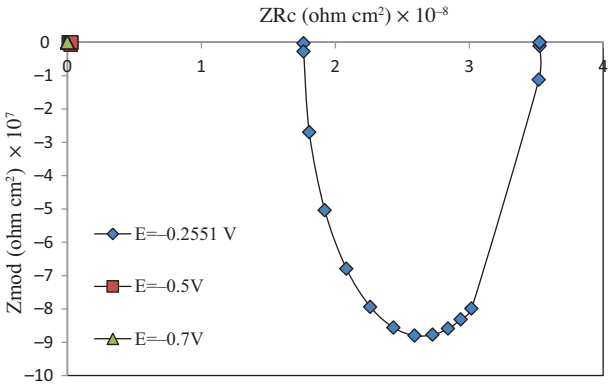

Figure 13. Nyquist plots showing the effect of reduction potential. Selected parameters for the simulation of impedance spectra: k = 9 × 10^{-22} cov^{-2} s^{-1}, C_{H+} = 0.5 M, Ea = 10,000 J/mol, C_{OX} = 0.5 M.

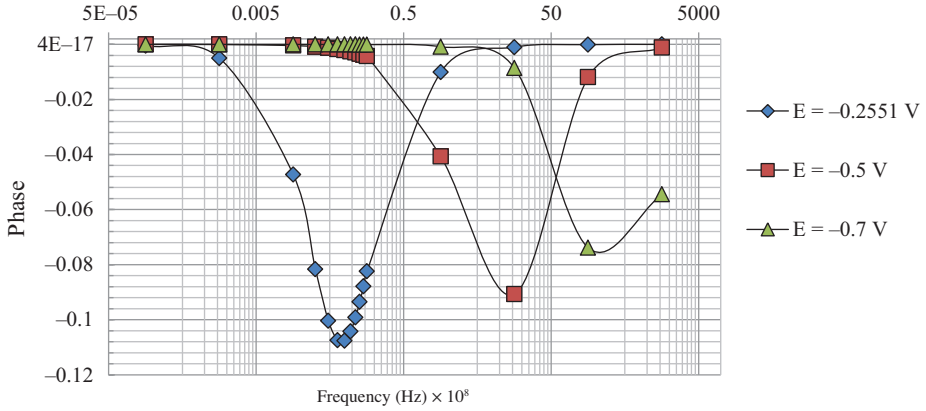

Figure 14. Bode plots showing the effect of reduction potential. Selected parameters for the simulation of impedance spectra: k = 9 × 10^{-22} cov^{-2} s^{-1}, C_{H+} = 0.5 M, Ea = 10,000 J/mol, C_{OX} = 0.5 M.

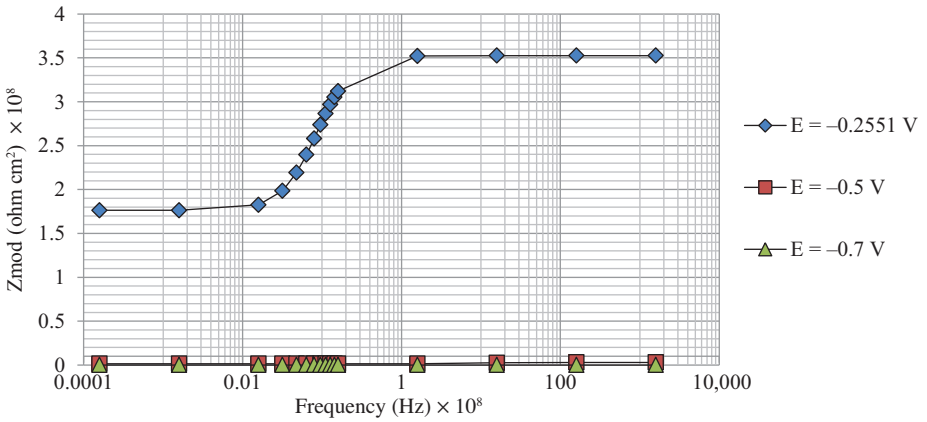

Figure 15. Modulus plots showing the effect of reduction potential. Selected parameters for the simulation of impedance spectra: k = 9 × 10^{-22} cov^{-2} s^{-1}, C_{H+} = 0.5 M, Ea = 10,000 J/mol, C_{OX} = 0.5 M.

Although the capacitive behaviors in both Figures 5 and 13 at low (C_{H+} = 5 × 10^{-5} M) and high proton concentrations (C_{H+} = 0.5 M) look similar, the depressed semicircles exhibit different shapes because the constant phase element parameters change.

The Bode plot in Figure 14 shows that the reduction in the capacitive behavior is more significant when the reduction potential becomes more negative. The modulus plot in Figure 15 clearly demonstrates a significant drop in the charge transfer resistance and capacitive behavior as the potential approaches –0.7 V. The effect of reduction potential on the impedance loop is also very similar to the case proton concentration because of the complex dependence of Ra, Ca, Rt, A1, and A2 on reduction potential (Eq. (15)) as discussed before. Figure 15 indicates purely resistive behavior at high reduction potentials (–0.5 and –0.7 V).

6. Conclusions

A 3-step mechanism was proposed for oxalic acid electroreduction to glyoxylic acid. The representative electrical circuit for the mechanism was determined to be composed of a DC path, 2 resistors, and a capacitance or inductance. The sign of overall matrix Q indicates the possibility of inductive behavior. After determination of a representative circuit for the proposed mechanism, the faradaic impedance equation based on 3 state variables was solved and the impedance spectra were analyzed. The results of the simulation indicate that increase in the alkyl chain length in the chemical activator decreases the charge transfer resistance slightly without changing capacitance in the faradaic impedance circuit. If the hydrogen evolution side reaction could be eliminated from the electroreduction mechanism, increasing proton concentration would have a drastic effect on the reduction in charge transfer resistance and capacitance. Inductive behavior was seen when the activation energy of the chemical step (ion transfer reaction) was lowered to 4 orders of magnitude. The occurrence of inductive behavior may be related to the limiting behavior of electroreduction of adsorbed oxalic acid. At higher negative potentials, the capacitive loop and charge transfer resistance diminish.

Nomenclature

C	Concentration, M
C_{OX}	Concentration of oxalic acid
E	Reduction potential, V
F	Faraday constant (C/mol equivalent)
I	Current, A
k	Pre-exponential factor
n	Number of equivalent
Y	Current efficiency
Z_{CPE}	Impedance of constant phase element, ohm cm^2
Z_f	Faradaic impedance, ohm cm^2
θ	Coverage

References

1. Scott, K. *Chem. Eng. Res. Des.* **1986**, *64*, 266–271.
2. Hamann, C. H.; Hamnett, A.; Vie, W. *Electrochemistry*, Wiley-VCH, Weinheim, 1998.
3. Zhou, Y. L.; Zhang, X. S.; Dai, Y. C.; Yuan, W.-K. *Chem. Eng. Sci.* **2003**, *58*, 1021–1027.
4. Gimenez, I.; Diard, J. P.; Maximovitch, B. L. G. S. *Electrochim. Acta* **1988**, *33*, 137–145.
5. Ahlberg, E.; Anderson, H. *Acta Chem. Scand.* **1992**, *46*, 1–14.
6. Scott, K. *Chem. Eng. Res. Des.* **1990,** *68*, 537–546.
7. Scott, K. *Electrochim. Acta* **1992**, *37*, 1381–1388.
8. Harrington, D. A.; van den Driessche, P. *J. Electroanal. Chem.* **2001**, *501*, 222–234.
9. Harrington, D. A. *J. Electroanal. Chem.* **1998**, *449*, 29.
10. Harrington, D.A.; van den Driessche, P. *Electrochim. Acta* **2011**, *56*, 8005– 8013.
11. Lasia, A. *In Electrochemical Impedance Spectroscopy and Its Applications, Modern Aspects of Electrochemistry*; Conway, B. E.; Bockris, J.; White, R. E., Eds.; Kluwer Academic/Plenum Publishers, NY, 1999.
12. Córdoba-Torresa, P.; Keddam, M; Nogueira, R. P. *Electrochim. Acta* **2008**, *54*, 518.
13. Córdoba-Torresa, P.; Keddam, M; Nogueira, R. P. *Electrochim. Acta* **2009**, 54, 6779.
14. Bockris, J. O'M.; Reddy, A. K. N. *Modern Electrochemistry*, Plenum Publishers, New York, 1999.
15. Macdonald, J. R. *J. Appl. Phys.* **1985**, 58, 1971–1978.
16. Macdonald, J. R. *J. Electroanal. Chem.* **1994**, *378*, 17–29.